Low- Z boundary of the N=88 –90 shape phase transition: Ce148 near the critical point

Koseoglou, P.; Werner, V.; Pietralla, N.; Ilieva, S.; Nikšić, T.; Vretenar, D.; Alexa, P.; Thürauf, M.; Bernards, C.; Blanc, A.; ...

Editors' Suggestion

Low-Z boundary of the $N = 88$–90 shape phase transition: ^{148}Ce near the critical point

P. Koseoglou,[1,2,*] V. Werner,[1,3] N. Pietralla,[1] S. Ilieva,[1] T. Nikšić,[4] D. Vretenar,[4] P. Alexa,[5] M. Thürauf,[1] C. Bernards,[3] A. Blanc,[6] A. M. Bruce,[7] R. B. Cakirli,[8] N. Cooper,[3] L. M. Fraile,[9] G. de France,[10] M. Jentschel,[6] J. Jolie,[11] U. Köster,[6] W. Korten,[12] T. Kröll,[1] S. Lalkovski,[13] H. Mach,[14] N. Mărginean,[15] P. Mutti,[6] Z. Patel,[13] V. Paziy,[9] Zs. Podolyák,[13] P. H. Regan,[13,16] J.-M. Régis,[11] O. J. Roberts,[7] N. Saed-Samii,[11] G. S. Simpson,[17] T. Soldner,[6] C. A. Ur,[18,19] W. Urban,[6,20] D. Wilmsen,[10] and E. Wilson[21]

[1]*Institute for Nuclear Physics, Technische Universität Darmstadt, Schlossgartenstr. 9, 64289 Darmstadt, Germany*
[2]*GSI Helmoltzzentrum für Schwerionenforschung GmbH, Planckstr. 1, 64291 Darmstadt, Germany*
[3]*Department of Physics, Yale University, P.O. Box 208120, New Haven, Connecticut 06520-8120, USA*
[4]*Physics Department, Faculty of Science, University of Zagreb, 10000 Zagreb, Croatia*
[5]*Department of Physics and Institute of Clean Technologies, VŠB-Technical University Ostrava, 17. listopadu 15, CZ-708 00 Ostrava, Czech Republic*
[6]*Institut Laue-Langevin, 71 avenue des Martyrs, 38042 Grenoble Cedex 9, France*
[7]*SCEM, University of Brighton, Lewes Road, Brighton BN2 4GJ, United Kingdom*
[8]*Department of Physics, Istanbul University, Vezneciler, 34134 Istanbul, Turkey*
[9]*Universidad Complutense, Grupo de Fisica Nuclear, Fisicas Avda. Complutense, 28040 Madrid, Spain*
[10]*Grand Accélérateur National d'Ions Lourds (GANIL), CEA/DRF-CNRS/IN2P3, Bvd Henri Becquerel, 14076 Caen, France*
[11]*IKP, University Cologne, Zülpicher Str. 77, 50937 Cologne, Germany*
[12]*Irfu, CEA, Université Paris-Saclay, F-91191 Gif-sur-Yvette, France*
[13]*Department of Physics, University of Surrey, Surrey GU2 7XH Guildford, United Kingdom*
[14]*National Centre for Nuclear Research, ul. Hoża 69, Warsaw, Poland*
[15]*Horia Hulubei NIPNE, 77125 Bucharest, Romania*
[16]*Nuclear Metrology Group, National Physical Laboratory, Teddington, TW11 OLW, United Kingdom*
[17]*LPSC, Université Grenoble Alpes, 38026 Grenoble Cedex, France*
[18]*Dipartimento di Fisica, Universita di Padova, Via F. Marzolo 8, 35131 Padova, Italy*
[19]*ELI-NP, National, IFIN-HH30, Reactorului, 077125 Bucharest-Magurele, Romania*
[20]*Faculty of Physics, University of Warsaw, ul. Pasteura 5, 02-093, Warszawa, Poland*
[21]*INFN - Laboratori Nazionali di Legnaro, Vialle dell Universita 2, 35020 Legnaro, Italy*

(Received 29 October 2019; published 6 January 2020)

Excited states of the neutron-rich nucleus ^{148}Ce have been populated by neutron-induced fission of a ^{235}U target. Its electromagnetic decays were studied by means of γ-ray coincidence spectroscopy with fast-timing capabilities. Lifetimes of the 2_1^+ and 4_1^+ states of ^{148}Ce were obtained and their $E2$ decay rates deduced. The $B_{4/2} = B(E2; 4_1^+ \rightarrow 2_1^+)/B(E2; 2_1^+ \rightarrow 0_1^+)$ ratio indicates that ^{148}Ce is a transitional nucleus while the $N = 88/90$ shape phase transition evolves into a gradual change of nuclear deformation for proton numbers $Z < 60$.

DOI: 10.1103/PhysRevC.101.014303

I. INTRODUCTION

A quantum shape phase transition (QSPT) in atomic nuclei is characterized by a sudden change of the shape of the nucleus as a function of the control parameter, such as nucleon number or excitation energy. It occurs due to changes in the location of the nuclear potential minimum [1]. The shape phase transition from spherical to prolate deformed rotational nuclei in the even-even $N = 90$ isotones with $Z = 56$–66 attracted a lot of attention during the last 15 to 20 years [1–9].

The E(5) and the so-called X(5) critical-point symmetries (CPSs) are solutions of the geometrical Bohr-Hamiltonian describing nuclei at the critical points of the second- and first-order QSPTs, respectively [10,11]. E(5) is the CPS between the quadrupole vibrator and the soft triaxial rotovibrator and X(5) between the quadrupole vibrator and the axially symmetric rigid rotor.

The X(5) approximate solution for the CPS of the vibrator-to-rotor transition neglects the barrier between the two minima and considers the potential as a square-well in the variable β and a harmonic oscillator in γ. The $R_{4/2} = E(4_1^+)/E(2_1^+) = 2.9$ and the $B_{4/2} = B(E2; 4_1^+ \rightarrow 2_1^+)/B(E2; 2_1^+ \rightarrow 0_1^+) = 1.58$ values are benchmarks for a nucleus at the X(5) critical point [11]. Using the adopted

*pkoseoglou@ikp.tu-darmstadt.de

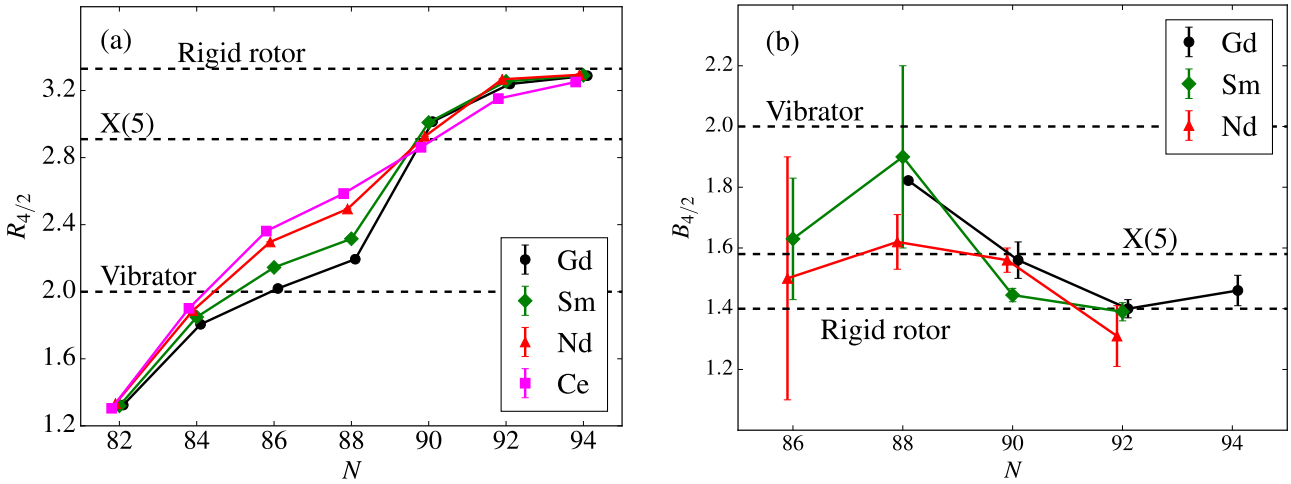

FIG. 1. (a) $R_{4/2}$ ratio for Gd, Sm, Nd, and Ce isotopic chains as a function of neutron number. The sharp transition of Gd and Sm from spherical nuclei ($R_{4/2} = 2$) to deformed ones ($R_{4/2} = 3.33$) is not present in Nd and Ce chains. (b) $B_{4/2}$ ratios for Gd, Sm, and Nd isotopic chains as a function of neutron number. The transition from $N = 88$ to $N = 90$ from near spherical symmetry to γ-rigid and γ-soft symmetry is sharp for Gd and Sm but not for Nd. Data taken from [12].

experimental data [12] for even-even nuclei in the nuclear region with neutron number $N \approx 90$, the discussed phase transition can be observed in a $R_{4/2}$ plot of these isotopes over the neutron number [Fig. 1(a)]. The transitions from spherical nuclei ($R_{4/2} = 2$–2.4) to deformed ones ($R_{4/2} = 3$–3.33) around $N = 90$ are less sharp in the neodymium and cerium chains as compared to the gadolinium and samarium isotopic chains [1,3,4].

To gain additional information on the shape of the nuclei, another fingerprint, the $B_{4/2}$ ratio ($B_{4/2} = 2.0$ for spherical symmetry, $B_{4/2} = 1.4$ for γ-rigid and γ-soft deformed), is shown in Fig. 1(b) as a function of the neutron number for gadolinium, samarium, and neodymium isotopes. In agreement with the picture from the $R_{4/2}$ ratios, the transition from $N = 88$ to $N = 90$ from near spherical symmetry to quadrupole deformed shapes is sharp for gadolinium and samarium and less so for neodymium. As indicated in Fig. 1, all fingerprints for quadrupole deformation of these $N = 90$ isotopes lie near the X(5) model [11], hence near the critical point of the QSPT.

Since the $R_{4/2}$ ratio evolution in the cerium isotopic chain is the most gradual in Fig. 1(a) it is of interest to study if X(5) is still imprinted in the $V_{4/2}$ value at $N = 90$, i.e., for ^{148}Ce. Unfortunately, no $B_{4/2}$ values are available experimentally in cerium isotopes with neutron number exceeding 84. It is the goal of this article to provide first experimental information on this structural key observable for ^{148}Ce.

II. EXPERIMENT AND ANALYSIS

Experimental data were provided from the EXILL&FATIMA campaign [13,14] which took place at the high-flux reactor at the Institut Laue-Langevin (ILL) in Grenoble, France. A well-collimated cold neutron beam was used to induce fission of a ^{235}U target. The neutron flux at the target position was approximately 9×10^7 n/cm^2 s [15,16]. Prompt γ rays from the fission fragments were detected using a hybrid array of HPGe and Ce-doped $LaBr_3$ detectors, the EXILL&FATIMA spectrometer [17,18]. The EXILL array [19] was composed of eight BGO-shielded EXOGAM Clover detectors [20], each one consisting of four HPGe crystals. The target-to-detector distance was 14.5 cm. FATIMA [21] consisted of 16 (5% Ce-doped) $LaBr_3$ detectors in two rings, at 40° and 140° relative to the beam direction. For optimum efficiency the FATIMA detectors were placed as close as possible to the target, at 8.5 cm. Several results for lifetimes in the picosecond and nanosecond region have already been published from the EXILL&FATIMA campaign [22–26]. A more detailed description of the experimental setup can be found in Ref. [17].

All fission fragments were stopped within few ps by the thick beryllium backing of the targets. More than 100 different isotopes were produced from the fissions. This large number of isotopes produced enforced the usage of multiple coincidences to select clean spectroscopy signals from the isotopes of interest. Ge-$LaBr_3$-$LaBr_3$ triple coincidences were used to gate on the cascade of interest. Because of the low energy resolution of the $LaBr_3$ detectors, the purity of the $LaBr_3$ gates had to be verified. Ge-Ge double coincidences or Ge-Ge-Ge and Ge-$LaBr_3$-Ge triple coincidences were studied for this purpose.

The 16 $LaBr_3$ detectors were connected to 15 time-to-amplitude converters (TACs). The connection scheme allowed to know which of the two prompt γs (decay or feeder of the state of interest) was the one providing the start signal and which providing the stop signal. Two time-difference spectra were produced depending on whether the transition decaying from the intermediate state of interest provided the *start* (antidelayed spectrum) or *stop* (delayed spectrum) signal.

In the case of a long-lived state, in the few-nanoseconds region, a slope appears on one side of the spectrum corresponding to the lifetime. For lifetimes in the order of some picoseconds the "center of gravity" [27], centroid, can be used. In the start spectrum the centroid ($Cstart$) is shifted to smaller

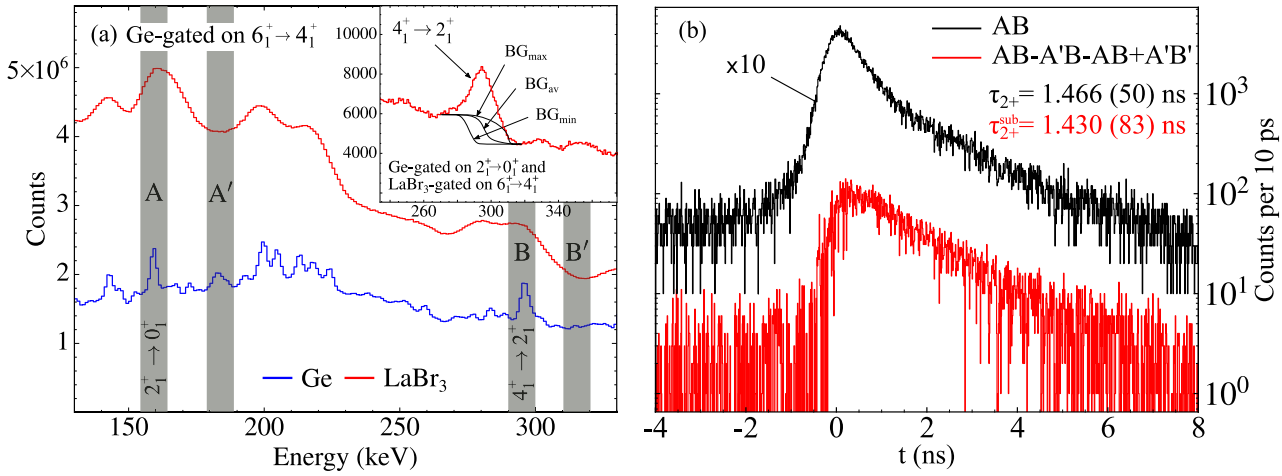

FIG. 2. (a) Energy spectra from the EXILL&FATIMA array gated on the $6_1^+ \rightarrow 4_1^+$ transition of ^{148}Ce in EXILL, Ge [blue (lower)] and $LaBr_3$ [red (upper)]. The gates in FATIMA detectors are marked with light gray. Combinations of those were set in order to get the time-difference spectra for the lifetime. The inset spectra ($LaBr_3$) is generated by setting an energy gate on the EXILL detectors on the $2_1^+ \rightarrow 0_1^+$ transition and an energy gate on the FATIMA detectors on the $6_1^+ \rightarrow 4_1^+$ transition. Three possible backgrounds under the full-energy peak are shown. (b) The black curve corresponds to the time-difference spectrum obtained from gates A and B, with the delayed and reflected antidelayed spectra summed in order to accommodate the full statistics. The red curve depicts the background-subtracted time-difference spectrum, with the delayed and the reflected antidelayed spectra summed up. Note that the black curve is multiplied by a factor of 10 for better visibility.

times by the lifetime of the intermediate state, while in the stop spectrum the centroid (*Cstop*) is shifted correspondingly to larger times. In the generalized centroid difference method (GCDM) [28] the lifetime of the intermediate state derives from the centroid difference (ΔC),

$$\Delta C = \mathrm{PRD} + 2\tau, \tag{1}$$

where the prompt response difference (PRD)

$$\begin{aligned} \mathrm{PRD} &= \mathrm{PRD}(\mathrm{E_{feeder}} - \mathrm{E_{decay}}) \\ &= \mathrm{PRF}(\mathrm{E_{feeder}}) - \mathrm{PRF}(\mathrm{E_{decay}}), \end{aligned} \tag{2}$$

and, in particular, the prompt response function (PRF) is reflecting the different time that the setup requires to record γs with different energies (the so-called *"time walk"*). The PRD was determined with known cascades from a ^{152}Eu source and the neutron-capture reaction ^{48}Ti$(n,\gamma)^{49}$Ti. A precise description of the procedure is given in Ref. [29].

A. 2_1^+ lifetime using the slope method

To derive the lifetime of the order of ns of the 2_1^+ state of ^{148}Ce, the slope method [30,31] was used. In order to preselect the isotope of interest an energy gate was set in the $6_1^+ \rightarrow 4_1^+$ transition in the EXILL Ge detectors. To obtain the time-difference spectra between the $4_1^+ \rightarrow 2_1^+$ and $2_1^+ \rightarrow 0_1^+$ γ rays, coincidence gates, A and B, as shown in Fig. 2(a), were set on the respective transitions. Using this method, the lifetime was measured to be $\tau_{2^+} = 1.466$ (50) ns, the average of the fitted slopes in both, the delayed and the antidelayed spectra.

The gates used include γ rays from the background, e.g., Compton events from higher-lying transitions. Therefore, the assumption must be made that lifetimes of states creating this background are in the ps region and do not affect the slope which has been fitted far away from the prompt response region. In order to check if that assumption is true, the method from Ref. [31] was used to exclude the time background contribution. The corresponding background gates, A′ and B′, are shown in Fig. 2(a). This method results in a lifetime of $\tau_{2^+}^{\mathrm{sub}} = 1.430$ (83) ns, hence, within error, in the same value as τ_{2^+} and reassures that no long-lived states contributed to the background. In Fig. 2(b) the time-difference spectra (sum of delayed and antidelayed), for both methods are shown. The measured lifetime is in agreement with the literature values of 1.457 (87) ns [32] and 1.371 (29) ns [33].

B. 4_1^+ lifetime using the generalized centroid difference method

For the 4_1^+ state the GCDM was used to determine the lifetime (in the ps range). The energy gate in the EXILL Ge detectors was set to the $2_1^+ \rightarrow 0_1^+$ transition of ^{148}Ce. In this case the FATIMA gates were set on the $6_1^+ \rightarrow 4_1^+$ and $4_1^+ \rightarrow 2_1^+$ transitions. The centroid difference of the delayed and antidelayed spectra was measured to $\Delta C_{\mathrm{exp}} = 66$ (3) ps. The spectra are shown in Fig. 3(a).

As it can be seen in the inset spectra of Fig. 2(a), generated by setting an energy gate on the EXILL detectors on the $2_1^+ \rightarrow 0_1^+$ transition and an energy gate on the FATIMA detectors on the $6_1^+ \rightarrow 4_1^+$ transition, there is a Compton-edge underneath the full-energy peak of the $4_1^+ \rightarrow 2_1^+$ transition. The exact location of the Compton edge is not known. Therefore, two extreme background assumptions [$\mathrm{BG_{max}}$, $\mathrm{BG_{min}}$ in Fig. 2(a)] were made, and an average of both [$\mathrm{BG_{av}}$ in Fig. 2(a)] used for the analysis, including a systematic error from the deviation to the extremes.

The contribution of the background in the time spectrum on the location of the full-energy peak can be found by the interpolation of the timing of the Compton background [17].

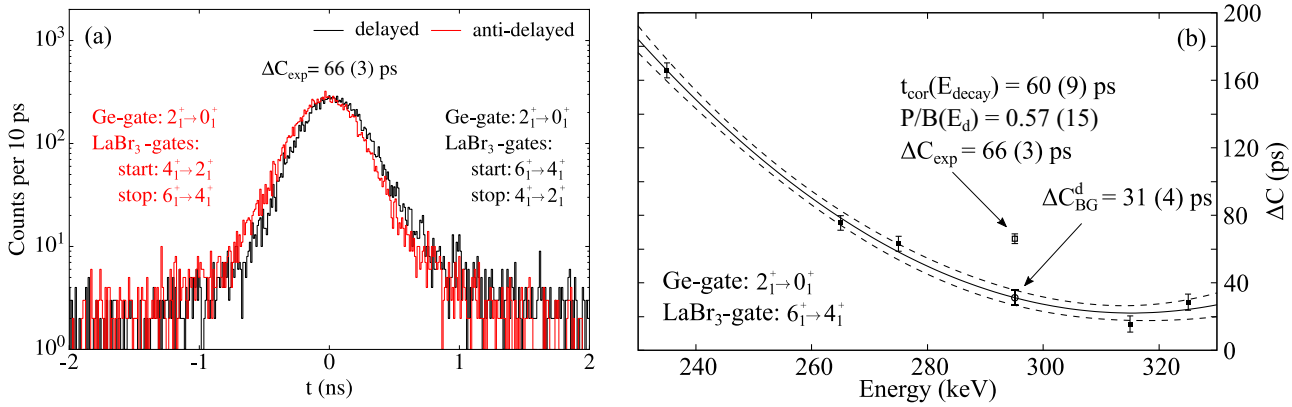

FIG. 3. (a) The time-difference spectra (delayed and antidelayed) for the lifetimes of the 4_1^+ states of ^{148}Ce. (b) The time-background under the full-energy peak of the $4_1^+ \rightarrow 2_1^+$ transition was interpolated from background areas around the peak (see text).

With this time background correction the ΔC in Eq. (1) has to be corrected by a correction factor ($t_{\rm cor}$). It will be

$$\Delta C = \Delta C_{\rm exp} + t_{\rm cor} = {\rm PRD} + 2\tau, \tag{3}$$

where

$$t_{\rm cor} = \frac{t_{\rm cor}(E_{\rm feeder}) + t_{\rm cor}(E_{\rm decay})}{2} \tag{4}$$

with

$$t_{\rm cor}(E_{f/d}) = \frac{\Delta C_{\rm exp} - \Delta C_{\rm BG}^{f/d}}{P/B(E_{f/d})}, \tag{5}$$

where $\Delta C_{\rm BG}$ is the interpolated background timing in the location of the full-energy peak and P/B is the peak-to-background ratio of the full-energy peak. In Fig. 3(b) the interpolation of the time-background for the $t_{\rm cor}(E_{\rm decay})$ is shown. Using Eq. (3) the lifetime of the 4_1^+ state of ^{148}Ce was measured to be $\tau_{4^+} = 58$ (4) ps.

III. RESULTS AND DISCUSSION

From the measured lifetimes the $B(E2; 2_1^+ \rightarrow 0_1^+)$ and $B(E2; 4_1^+ \rightarrow 2_1^+)$ transition strengths were determined to be 85.2 (29) W.u. and 129.7 (86) W.u. respectively, which results in a ratio of Eq. (11). All experimental results are summarized in Table I. The ratio deviates from both the vibrational and the rotor's values, setting the nucleus, together with its heavier $N = 90$ isotones, in the transitional region as it is shown in Fig. 4(a).

In order to understand the QSPT, in the following paragraphs the experimental data for ^{148}Ce will be compared with

TABLE I. Lifetimes and transition strengths in ^{148}Ce obtained from the present work.

J_i^π	τ	τ - lit.	J_f^π	$B(E2; J_i^\pi \rightarrow J_f^\pi)$
2_1^+	1.466 (50) ns	1.457 (87) ns [32] 1.371 (29) ns [33]	0_1^+	85.2 (29) W.u.
4_1^+	58 (4) ps		2_1^+	129.7 (86) W.u.

(a) several geometrical models approximating the transitional region around X(5), and (b) microscopic calculations for this nucleus using the five-dimensional quadrupole collective Hamiltonian, Eq. (9). Additionally the whole transitional region is being investigated with interacting boson model (IBM)-1 calculations. The trajectories of cerium, neodymium, and samarium isotopic chains in the IBM symmetry triangle are showing the different crossing of the phase boundary of the QSPT.

A. Geometrical models

Besides X(5) there are other analytical solutions of the Bohr Hamiltonian with soft potentials in the deformation variable β. The X(5)-β^{2n} model [34] was introduced to describe the spherical side of the QSPT. With $n = 1$, X(5)-β^2, the nuclear potential is the harmonic oscillator (vibrator) and with increasing n the potentials of the model approach the infinite square-well of X(5). The confined β-soft model (CBS) [4] considers an infinite square-well potential between minimum and maximum deformation, $\beta_<$ and $\beta_>$, with its structural parameter $r_\beta = \beta_</\beta_>$. For different widths of the potential well the model describes nuclei between X(5) and the rigid rotor.

The adopted experimental data for ^{148}Ce are presented in Table II together with the observables of the X(5) and X(5)-β^8. The calculations were taken from Refs. [11,34]. One can perceive the good agreement of ^{148}Ce with the X(5)-β^8 model. This agreement can also be clearly seen in Fig. 4(b) where the energy ratios $E(J^+)/E(2^+)$ with $J \leqslant 14$, are plotted for a vibrator, a rigid rotor, X(5) and X(5)-β^8 models and the experimental data of ^{148}Ce. The experimental data fit with high precision with the X(5)-β^8 model.

The comparison of the experimental data for ^{148}Ce with the geometrical models places the nucleus before the critical point of the QSPT where the spherical minimum still dominates the structure. In all above-mentioned models [X(5), X(5)-β^{2n} and CBS] the γ degree of freedom is separated and approximated by a harmonic oscillator centered around $\gamma = 0^\circ$. None of these geometrical models have predictive power for the

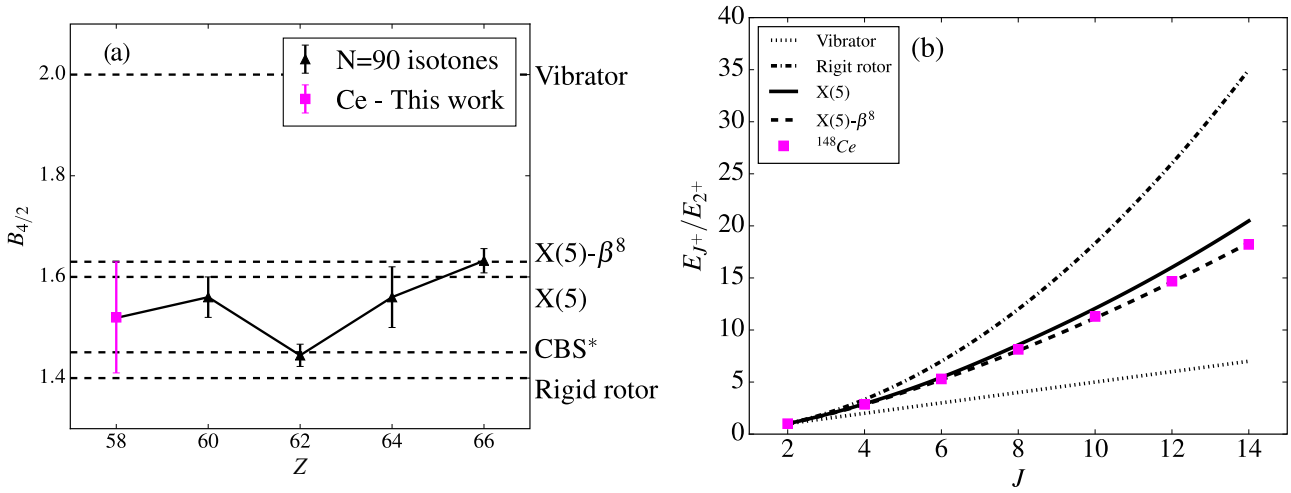

FIG. 4. (a) The $B_{4/2}$ ratio for $N = 90$ isotopes. All isotopes lie near the QSPT with the exception of ^{152}Sm which deviates towards the rigid rotor. Data taken from [12].*The CBS line is adjusted to the experimental $R_{4/2}$ ratio of ^{152}Sm with $r_\beta = 0.14$ [4]. (b) Energy ratios of ^{148}Ce. Comparison of experimental data with vibrator, rigid rotor, X(5) and X(5)-β^8 models.

excitation energy of the 2^+_γ state. In the next paragraphs the γ dependence of ^{148}Ce will be investigated within the IBM-1.

B. IBM-1 model

In the context of the present discussion we adopt the standard extended constant Q formalism (ECQF) [35,36] of the IBM-1 with the Hamiltonian

$$H = c\left[(1-\zeta)\hat{n}_d - \frac{\zeta}{4N_B}\hat{Q}^\chi \cdot \hat{Q}^\chi\right], \qquad (6)$$

where

$$\hat{Q}^\chi = (s^\dagger \tilde{d} + d^\dagger \tilde{s}) + \chi(\tilde{d}d^\dagger)^{(2)} = T(E2)/e_B, \qquad (7)$$

is the quadrupole operator, $T(E2)$ is the electric quadrupole transition operator with the effective boson charge e_B, c is a scaling factor, and N_B the number of valence bosons. In Eq. (6) the quadrupole-quadrupole interaction drives deformation and the parameter ζ controls the competition between the spherical-driving and deformed-driving forces [3]. With the parameters ζ and χ the standard IBM symmetry triangle [37] can be mapped, with $\zeta \in [0, 1]$ and $\chi \in [-\sqrt{7}/2, 0]$, see Fig. 5. The parameter ζ mainly controls the β deformation while γ has a strong χ dependence. Spherical nuclei are described by small ζ. As ζ increases the nucleus can undergo a spherical-to-deformed QSPT [38].

Following the concept of the Ehrenfest classification [39] in Ref. [40] derivatives of observables were used to determine the critical points (CPs) of the QSPT in a finite-N system, over different/constant χ parameters. In the present work the CPs are determined by the second derivative of the binding energy. The slope of the binding energy is the order parameter of the many-body system. The calculations have been made with the code IBAR which performs interacting boson model-1 (IBM-1) calculations [41].

For each boson number and χ parameter the maximum of the second derivative of the binding energy defines the location of the shape phase transitional point as a function of ζ: $\zeta_{\rm QSPT}(N_B, \chi)$ [42]. These trajectories as a function of χ, for now on referred to as phase transition lines (PT lines), are plotted for various boson numbers of interest over the IBM

TABLE II. Comparison between experimental data of ^{148}Ce with geometrical models, the $\zeta_{\rm QSPT}(8, -0.943)$ from the IBM (see Sec. III B) and microscopic calculations (see Sec. III C).

	X(5)	X(5)-β^8	$\zeta_{\rm QSPT}$ (8, −0.94)	5DQCH	^{148}Ce Exp.
$R_{4/2}$	2.90	2.85	2.59	2.99	2.86
$E_{0^+_2}/E_{2^+_1}$	5.65	5.09	3.29	5.21	4.86
$E_{2^+_\gamma}/E_{2^+_1}$			5.59	5.85	6.24
$B_{4/2}$	1.6	1.63	1.55	1.54	1.52 (11)

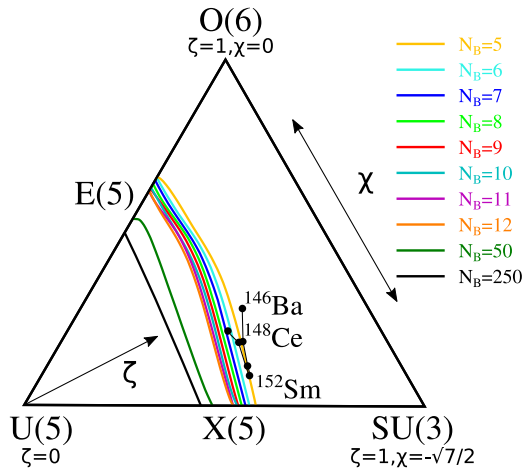

FIG. 5. PT lines for several boson numbers, 5–12, 50, and 250. For increasing boson number the PT line moves towards smaller values of ζ (from right to left for increasing boson number).

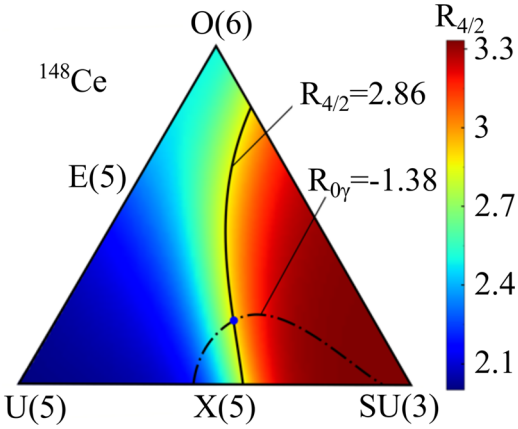

FIG. 6. Placement of ^{148}Ce into the IBM symmetry triangle of the IBM. The two contours ($R_{4/2}$ and $R_{0\gamma}$) fitting the experimental data are shown.

symmetry triangle in Fig. 5. Note that for small N_B and to a lesser extent for small χ values the maximum in the second derivative of the binding energy is less pronounced indicating that the spherical-to-deformed transition is less sudden. The trajectories divide the triangle in two areas each. Take note of the fact that this division into the spherical region and the deformed region depends on the boson number.

The IBM-1 calculations for various ζ and χ parameters provide observables along the triangle including those in Table II. These experimental data can be used for the placement of isotopes in the triangle [43–46]. It is known that the $R_{4/2}$ ratio is very sensitive to the stiffness of the potential in the quadrupole deformation parameter β. For a given stiffness in β, the stiffness of the potential as a function of the γ deformation parameter is correlated with the energy difference between the first excited 0^+ state and the 2^+_γ state. The $R_{4/2}$ contours have a vertical trajectory (with respect to the base of the triangle), and the

$$R_{0\gamma} = \frac{E(0^+_2) - E(2^+_\gamma)}{E(2^+_1)}, \tag{8}$$

proposed in Ref. [45], have a more horizontal trajectory. For all the isotopes in the QSPT region the crossing of the two contours is unique and allows their unique placement in the triangle.

In Fig. 6 the placement of ^{148}Ce is shown. For ^{148}Ce the experimental data for the two observables are $R_{4/2} = 2.86$ and $R_{0\gamma} = -1.38$ simultaneously corresponding to the coordinates $\zeta = 0.64$ and $\chi = -0.94$. The same method has been used in order to define the trend of the Ce isotopic chain within the triangle. In Fig. 7(a) the placement of the even-even Ce isotopes with $N = 86$–90 is shown together with the PT lines for the corresponding valence boson numbers $N_B = 6$–8. For ^{144}Ce the energy of the 0^+_2 state is not known experimentally, so the curve inside the triangle where it is placed was defined only by $R_{4/2}$. The ^{146}Ce isotope is placed on the spherical side of the PT line for $N_B = 7$ and ^{148}Ce on the deformed side of the PT line for $N_B = 8$. Note the dependence of the nucleus' shape assignment on the finite boson number for which the PT line was calculated. The experimental data for ^{148}Ce are compared in Table II to the IBM-1 observables for the CP obtained as a function of ζ for the fixed structural parameter $\chi = -0.94$. Indeed, the observed $R_{4/2}$ ($B_{4/2}$) ratio for ^{148}Ce exceeds (is smaller than) the value expected at the PT point for this appropriate structural parameter and boson number $N_B = 8$, unambiguously placing ^{148}Ce in the deformed part of the IBM symmetry triangle. We conclude that *the spherical-to-deformed phase transition in cerium isotopes happens between* ^{146}Ce *and* ^{148}Ce. The locations of the cerium isotopes evolving to larger values of χ as a function of mass imply an increasing role of the γ degree of freedom.

For a further analysis of the proton number dependence of the $N \approx 90$ QSPT we apply this procedure to the neodymium

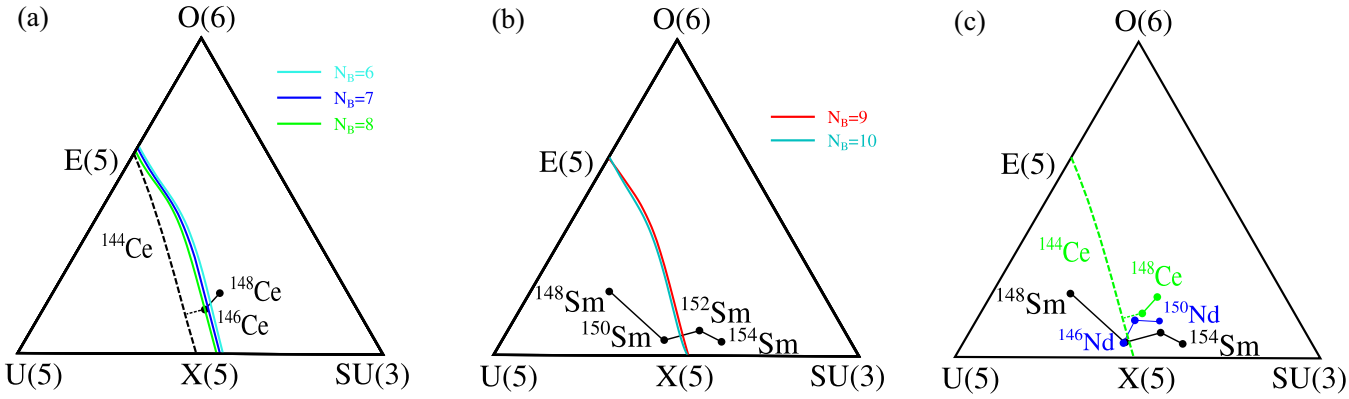

FIG. 7. Trajectories of (a) cerium and (b) samarium isotopes in the IBM symmetry triangle. For ^{144}Ce the observable R_γ is unknown hence its $R_{4/2}$ contour is shown with a dashed line which is located entirely on the spherical side of the PT line. ^{144}Ce is classified as spherical. The PT lines corresponding to the valence boson number of the isotopes are also plotted (from right to left for increasing boson number). (c) Comparison of the trajectories of the cerium, neodymium, and samarium isotopic chains inside the triangle as a function of neutron number.

TABLE III. Coordinates of isotopes in the IBM symmetry triangle. *The placement of ^{144}Ce in one spot was not possible in the procedure adopted here, because the energy of the 0_2^+ is not known experimentally. The isotope was placed on a curve instead, using only the energy ratio $R_{4/2}$.

Isotope	ζ	χ	$N = 90$ isotones	ζ	χ
^{144}Ce*	0.5 to 0.6	0 to $-\sqrt{7}/2$	^{146}Ba	0.69	−0.78
^{146}Ce	0.59	−1.02	^{148}Ce	0.64	−0.94
^{146}Nd	0.50	−1.17	^{150}Nd	0.62	−1.08
^{148}Nd	0.56	−1.04	^{152}Sm	0.61	−1.13
^{148}Sm	0.43	−0.68	^{154}Gd	0.63	−0.93
^{150}Sm	0.51	−1.14	^{156}Dy	0.62	−0.87
^{154}Sm	0.65	−1.23			

and samarium isotopic chains. The placement of the even-even samarium isotopes [with $N = 86$–92] into the triangle [see Fig. 7(b)] reveals the lower dependence on the γ degree of freedom of these isotopes. Again the crossing from the spherical side to the deformed side of the PT line is between the $N = 88$ and $N = 90$ isotopes, like in the cerium isotopic chain. The QSPT in the samarium chain occurs at smaller values of χ than in the cerium chain. The same picture occurs for the neodymium chain. In this case the χ parameter at the QSPT lies between the one for cerium and samarium [see Fig. 7(c)]. It seems that by decreasing Z, from samarium to cerium, the dependence on the γ degree of freedom increases at the $N \approx 90$ QSPT. The coordinates of all isotopes discussed before are included in Table III.

Both in the limit of the large boson number and in the small finite boson number the QSPT has a pronounced phase transition behavior only for small χ parameters. As χ increases, approaching zero, the phase transition washes out. The samarium isotopic chain is crossing the PT lines (for $N_B = 9$ and 10, corresponding to ^{150}Sm and ^{152}Sm) almost perpendicularly at small χ parameters. This implies a more sudden change in the shape of the nuclei in the samarium isotopic chain than in the cerium chain. The cerium isotopic chain is crossing the PT lines (for $N_B = 7$ and 8, corresponding to ^{146}Ce and ^{148}Ce) at larger and increasing χ parameters thus the transition from spherical to deformed shapes is smoother and involves higher dependence on the γ degree of freedom.

All the $N = 90$ isotones are placed on the deformed side of their corresponding PT line as seen in Fig. 5. In Fig. 8 the energy spectra of the $N = 90$ isotones are plotted, the 0_2^+ state and the 2_γ^+ state are also included. The energy of the 2_γ^+ level peaks in ^{152}Sm, indicating its highest degree of axial symmetry, also reported in Ref. [47].

C. Microscopic calculations

The contradicting shape assignment of ^{148}Ce when its level scheme is compared with the observables of the geometrical models and when it is compared with the IBM calculations motivate further microscopic calculations for the nucleus. Axial Skyrme-Hartree-Fock-Bogoliubov (Skyrme-HFB) [48] calculations (Skyrme interaction parametrization

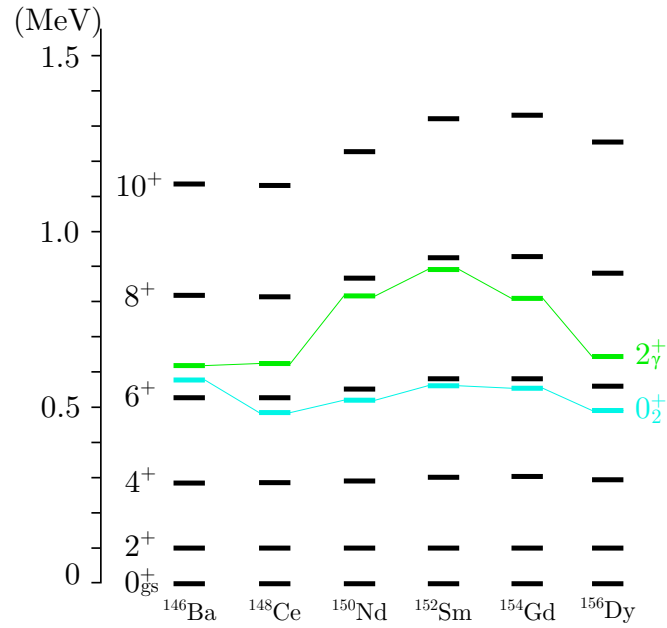

FIG. 8. Comparison of energy spectra of the adopted experimental data for $N = 90$ isotones. The energies of the levels of each isotope are normalized to the energy of the 2_1^+ state which is shifted to 100 keV. The 0_2^+ states are plotted with light blue and the 2_γ^+ states are plotted with green. The trend of the 2_γ^+ shows an decreasing γ-softness around ^{152}Sm.

SVmin [49,50]) were performed resulting in a shallow minimum $\beta_2 = 0.248$ with a potential energy curve bump characteristic for nuclei close to X(5) [51]. Beyond mean field full-Skyrme random phase approximation (RPA) calculations predict correct 2_1^+ energy of 158 keV [52] and $B(E2; 2_1^+ \rightarrow 0_1^+) = 84$ W.u. in agreement with the experimental value.

Another recently introduced [53] approach makes use of the five-dimensional quadrupole collective Hamiltonian (5DQCH)

$$\hat{H}_{\rm coll} = \hat{T}_{\rm vib} + \hat{T}_{\rm rot} + V_{\rm coll} \tag{9}$$

as described in Ref. [53]. In the past the microscopic framework of the 5DQCH was used for the analysis of the QSPT in the $N = 90$ isotones for neodymium, samarium, and gadolinium [7,8].

In Fig. 9(a) the potential energy surface of ^{148}Ce is plotted. The equilibrium minimum (red dot) is located at $\beta \approx 0.25$ (and $\gamma = 0$, prolate). In comparison with the results, in Ref. [53], for ^{152}Sm, ^{154}Gd, and ^{156}Dy the β deformation is the smallest in ^{148}Ce. The extended potential minimum indicates significant γ-softness. Additionally, the collective wave functions, plotted in Fig. 9(b)–9(f), appear to display mixing in the γ direction. So the scenario of the γ-softness in ^{148}Ce is supported by the microscopic calculations.

The agreement with the experimental data can bee seen in Table II where the observables emanating from the calculations are shown next to the experimental values for ^{148}Ce. The transition strengths, $B(E2; 2_1^+ \rightarrow 0_1^+)$ and $B(E2; 4_1^+ \rightarrow 2_1^+)$, agree with the experiment: The 5DQCH approach results in $B(E2; 2_1^+ \rightarrow 0_1^+) = 80$ W.u. and $B(E2; 4_1^+ \rightarrow 2_1^+) = 123$ W.u. (cf. Table I).

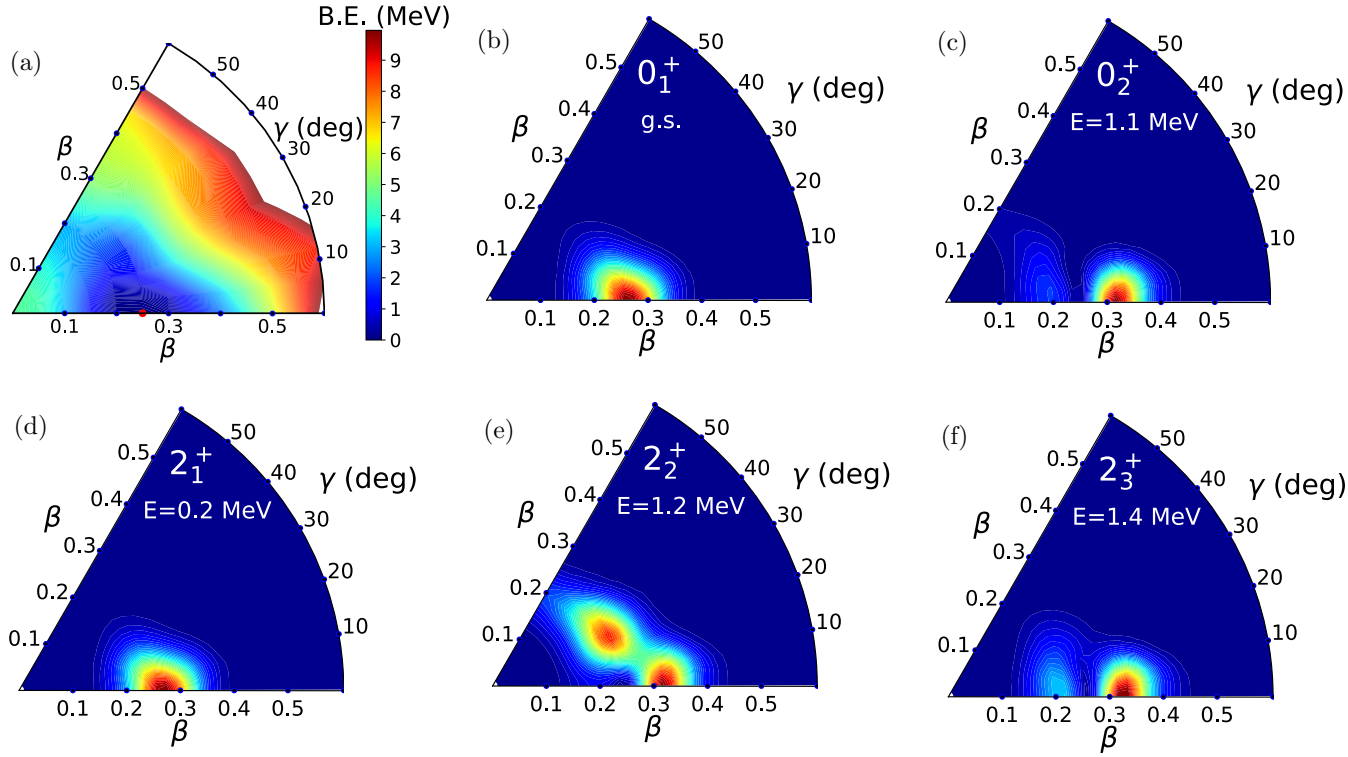

FIG. 9. (a) Self-consistent triaxial quadrupole constrained energy surfaces in the β-γ plane($0 \leqslant \gamma \leqslant 60^\circ$). (b–f) Probability distributions in the β-γ plane for the wave function of the lowest collective 0^+ and 2^+ states of ^{148}Ce.

IV. CONCLUSION

The lifetimes of the 2_1^+ and 4_1^+ states of ^{148}Ce were measured with fast electronic timing. The $B_{4/2}$ value was extracted for the first time. It agrees with a new view on the structure of the nucleus and the evolution of the QSPT along the $N = 90$ line. Although the basic structural observables, in particular energy ratios, compare favorably to the X(5)-β^8 model mimicking dominant sphericity of ^{148}Ce, a deeper analysis which takes the finite size of the quantum system and the γ-degree of freedom into account implies that ^{148}Ce is actually deformed. The evolution of the QSPT at $N = 90$ is smoothed out as a function of decreasing proton number due to finite-N effects and increasing γ-softness.

ACKNOWLEDGMENTS

We are grateful to F. Iachello, R. F. Casten, and D. Bonatsos for useful discussions. The EXILL&FATIMA campaign would not have been possible without the support of several services at the ILL and the LPSC. We are grateful to the EXOGAM collaboration for the loan of the detectors, to GANIL for assistance during installation and dismantling, and to the FATIMA collaboration for the provision of $LaBr_3$ (Ce) detectors and analog electronics. This work was supported by the cooperation between TU Darmstadt and the GSI Helmholtz Center for Heavy Ion Research and by the Helmholtz Graduate School for Hadron and Ion Research for FAIR, by the QuantiXLie Centre of Excellence, a project co-financed by the Croatian Government and European Union through the European Regional Development Fund - the Competitiveness and Cohesion Operational Programme (Grant No. KK.01.1.1.01), by US DOE under Grant No. DE-FG02-91ER-40609, by UK Science and Technologies Facilities Council (STFC) under Grants No. ST/L005743/1, No. ST/G000751/1, No. ST\L\0057\1, and No. ST\P005314\1, by Istanbul University Scientific Research Project No. 54135, by DFG under Grants No. KR 1796/2-1,2 and No. SFB1245 and by BMBF under Grants No. 05P12RDNUP, No. 05P(15/19)RDFN1, No. 05P(15/19)PKFNA, and No. 05P12PKNUF. P.H.R. acknowledges partial support from the UK Department of Business, Energy and Industrial Strategy (BEIS) via the National Measurement System (NMS). P.A. acknowledges support from SP2018/84 and LO1406 projects.

[1] R. F. Casten and N. V. Zamfir, Phys. Rev. Lett. **87**, 052503 (2001).
[2] D. Warner, Nature **420**, 614 (2002).
[3] R. F. Casten, Nat. Phys. **2**, 811 (2006).
[4] N. Pietralla and O. M. Gorbachenko, Phys. Rev. C **70**, 011304(R) (2004).
[5] R. Krücken, B. Albanna, C. Bialik, R. F. Casten, J. R. Cooper, A. Dewald, N. V. Zamfir, C. J. Barton, C. W. Beausang,

M. A. Caprio, A. A. Hecht, T. Klug, J. R. Novak, N. Pietralla, and P. von Brentano, Phys. Rev. Lett. **88**, 232501 (2002).
[6] D. Tonev, A. Dewald, T. Klug, P. Petkov, J. Jolie, A. Fitzler, O. Möller, S. Heinze, P. von Brentano, and R. F. Casten, Phys. Rev. C **69**, 034334 (2004).
[7] T. Nikšić, D. Vretenar, G. A. Lalazissis, and P. Ring, Phys. Rev. Lett. **99**, 092502 (2007).
[8] Z. P. Li, T. Nikšić, D. Vretenar, J. Meng, G. A. Lalazissis, and P. Ring, Phys. Rev. C **79**, 054301 (2009).
[9] J. Wiederhold, R. Kern, C. Lizarazo, N. Pietralla, V. Werner, R. V. Jolos, D. Bucurescu, N. Florea, D. Ghita, T. Glodariu, R. Lica, N. Marginean, R. Marginean, C. Mihai, R. Mihai, I. O. Mitu, A. Negret, C. Nita, A. Olacel, S. Pascu, L. Stroe, S. Toma, and A. Turturica, Phys. Rev. C **94**, 044302 (2016).
[10] F. Iachello, Phys. Rev. Lett. **85**, 3580 (2000).
[11] F. Iachello, Phys. Rev. Lett. **87**, 052502 (2001).
[12] Nuclear Data Sheets, http://www.nndc.bnl.gov/ensdf/.
[13] D. Biswas, E. Clement, G. de France, L. M. Fraile, J. Jolie, T. Kröll, S. Lalkovski, S. Leoni, R. Lozeva, P. Regan *et al.*, ILL-DATA (2013).
[14] D. Balabanski, D. Biswas, I. Celikovic, E. Clement, G. de France, F. Drouet, G. Gey, J. Kurpeta, S. Leoni, O. Litaize *et al.*, ILL-DATA (2013).
[15] H. Abele, D. Dubbers, H. Häse, M. Klein, A. Knöpfler, M. Kreuz, T. Lauer, B. Märkisch, D. Mund, V. Nesvizhevsky, A. Petoukhov, C. Schmidt, M. Schumann, and T. Soldner, Nucl. Instrum. Methods Phys. Res. A **562**, 407 (2006).
[16] W. Urban, M. Jentschel, B. Märkisch, T. Materna, C. Bernards, C. Drescher, C. Fransen, J. Jolie, U. Köster, P. Mutti, T. Rząca-Urban, and G. S. Simpson, J. Instrum. **8**, P03014 (2013).
[17] J.-M. Régis, G. Simpson, A. Blanc, G. de France, M. Jentschel, U. Köster, P. Mutti, V. Paziy, N. Saed-Samii, T. Soldner, C. Ur, W. Urban, A. Bruce, F. Drouet, L. Fraile, S. Ilieva, J. Jolie, W. Korten, T. Kröll, S. Lalkovski, H. Mach, N. Mărginean, G. Pascovici, Z. Podolyák, P. Regan, O. Roberts, J. Smith, C. Townsley, A. Vancraeyenest, and N. Warr, Nucl. Instrum. Methods Phys. Res. Sec. A **763**, 210 (2014).
[18] J. Jolie, J.-M. Régis, D. Wilmsen, N. Saed-Samii, M. Pfeiffer, N. Warr, A. Blanc, M. Jentschel, U. Köster, P. Mutti, T. Soldner, G. Simpson, G. de France, W. Urban, F. Drouet, A. Vancraeyenest, A. Bruce, O. Roberts, L. Fraile, V. Paziy, A. Ignatov, T. Kröll, D. Ivanova, S. Kisyov, S. Lalkovski, Z. Podolyák, P. Regan, E. Wilson, W. Korten, C. Ur, R. Lica, and N. Marginean, Nucl. Phys. A **934**, 1 (2015).
[19] M. Jentschel, A. Blanc, G. de France, U. Köster, S. Leoni, P. Mutti, G. Simpson, T. Soldner, C. Ur, W. Urban, S. Ahmed, A. Astier, L. Augey, T. Back, P. Baączyk, A. Bajoga, D. Balabanski, T. Belgya, G. Benzoni, C. Bernards, D. Biswas, G. Bocchi, S. Bottoni, R. Britton, B. Bruyneel, J. Burnett, R. Cakirli, R. Carroll, W. Catford, B. Cederwall, I. Celikovic, N. Cieplicka-Oryńczak, E. Clement, N. Cooper, F. Crespi, M. Csatlos, D. Curien, M. Czerwiński, L. Danu, A. Davies, F. Didierjean, F. Drouet, G. Duchêne, C. Ducoin, K. Eberhardt, S. Erturk, L. Fraile, A. Gottardo, L. Grente, L. Grocutt, C. Guerrero, D. Guinet, A.-L. Hartig, C. Henrich, A. Ignatov, S. Ilieva, D. Ivanova, B. John, R. John, J. Jolie, S. Kisyov, M. Krticka, T. Konstantinopoulos, A. Korgul, A. Krasznahorkay, T. Kröll, J. Kurpeta, I. Kuti, S. Lalkovski, C. Larijani, R. Leguillon, R. Lica, O. Litaize, R. Lozeva, C. Magron, C. Mancuso, E. R. Martinez, R. Massarczyk, C. Mazzocchi, B. Melon, D. Mengoni, C. Michelagnoli, B. Million, C. Mokry, S. Mukhopadhyay, K. Mulholland, A. Nannini, D. Napoli, B. Olaizola, R. Orlandi, Z. Patel, V. Paziy, C. Petrache, M. Pfeiffer, N. Pietralla, Z. Podolyak, M. Ramdhane, N. Redon, P. Regan, J. M. Régis, D. Regnier, R. J. Oliver, M. Rudigier, J. Runke, T. Rzaąca-Urban, N. Saed-Samii, M. Salsac, M. Scheck, R. Schwengner, L. Sengele, P. Singh, J. Smith, O. Stezowski, B. Szpak, T. Thomas, M. Thürauf, J. Timar, A. Tom, I. Tomandl, T. Tornyi, C. Townsley, A. Tuerler, S. Valenta, A. Vancraeyenest, V. Vandone, J. Vanhoy, V. Vedia, N. Warr, V. Werner, D. Wilmsen, E. Wilson, T. Zerrouki, and M. Zielinska, J. Instrum. **12**, P11003 (2017).
[20] J. Simpson, F. Azaiez, G. de France, J. Fouan, J. Gerl, R. Julin, W. Korten, P. J. Nolan, B. Nyakó, G. Sletten, and P. M. Walker, Acta Phys. Hung. A **11**, 159 (2000).
[21] FATIMA - FAst TIMing Array, http://nuclear.fis.ucm.es/fasttiming/index.html.
[22] J.-M. Régis, J. Jolie, N. Saed-Samii, N. Warr, M. Pfeiffer, A. Blanc, M. Jentschel, U. Köster, P. Mutti, T. Soldner, G. S. Simpson, F. Drouet, A. Vancraeyenest, G. de France, E. Clément, O. Stezowski, C. A. Ur, W. Urban, P. H. Regan, Z. Podolyák, C. Larijani, C. Townsley, R. Carroll, E. Wilson, L. M. Fraile, H. Mach, V. Paziy, B. Olaizola, V. Vedia, A. M. Bruce, O. J. Roberts, J. F. Smith, T. Kröll, A.-L. Hartig, A. Ignatov, S. Ilieva, M. Thürauf, S. Lalkovski, D. Ivanova, S. Kisyov, W. Korten, M.-D. Salsac, M. Zielińska, N. Mărginean, D. G. Ghită, R. Lică, C. M. Petrache, A. Astier, and R. Leguillon, Phys. Rev. C **90**, 067301 (2014).
[23] S. Ilieva, T. Kröll, J.-M. Régis, N. Saed-Samii, A. Blanc, A. M. Bruce, L. M. Fraile, G. de France, A.-L. Hartig, C. Henrich, A. Ignatov, M. Jentschel, J. Jolie, W. Korten, U. Köster, S. Lalkovski, R. Lozeva, H. Mach, N. Mărginean, P. Mutti, V. Paziy, P. H. Regan, G. S. Simpson, T. Soldner, M. Thürauf, C. A. Ur, W. Urban, and N. Warr, Phys. Rev. C **94**, 034302 (2016).
[24] P. Spagnoletti, G. S. Simpson, R. Carroll, J.-M. Régis, A. Blanc, M. Jentschel, U. Köster, P. Mutti, T. Soldner, G. de France, C. A. Ur, W. Urban, A. M. Bruce, F. Drouet, L. M. Fraile, L. P. Gaffney, D. G. Ghită, S. Ilieva, J. Jolie, W. Korten, T. Kröll, C. Larijani, S. Lalkovski, R. Lică, H. Mach, N. Mărginean, V. Paziy, Z. Podolyák, P. H. Regan, M. Scheck, N. Saed-Samii, G. Thiamova, C. Townsley, A. Vancraeyenest, V. Vedia, A. Gargano, and P. Van Isacker, Phys. Rev. C **95**, 021302(R) (2017).
[25] J.-M. Régis, J. Jolie, N. Saed-Samii, N. Warr, M. Pfeiffer, A. Blanc, M. Jentschel, U. Köster, P. Mutti, T. Soldner, G. S. Simpson, F. Drouet, A. Vancraeyenest, G. de France, E. Clément, O. Stezowski, C. A. Ur, W. Urban, P. H. Regan, Z. Podolyák, C. Larijani, C. Townsley, R. Carroll, E. Wilson, L. M. Fraile, H. Mach, V. Paziy, B. Olaizola, V. Vedia, A. M. Bruce, O. J. Roberts, J. F. Smith, M. Scheck, T. Kröll, A.-L. Hartig, A. Ignatov, S. Ilieva, S. Lalkovski, W. Korten, N. Mărginean, T. Otsuka, N. Shimizu, T. Togashi, and Y. Tsunoda, Phys. Rev. C **95**, 054319 (2017).
[26] S. Ansari, J.-M. Régis, J. Jolie, N. Saed-Samii, N. Warr, W. Korten, M. Zielińska, M.-D. Salsac, A. Blanc, M. Jentschel, U. Köster, P. Mutti, T. Soldner, G. S. Simpson, F. Drouet, A. Vancraeyenest, G. de France, E. Clément, O. Stezowski, C. A. Ur, W. Urban, P. H. Regan, Z. Podolyák, C. Larijani, C. Townsley, R. Carroll, E. Wilson, H. Mach, L. M. Fraile, V. Paziy, B. Olaizola, V. Vedia, A. M. Bruce, O. J. Roberts, J. F. Smith, M. Scheck, T. Kröll, A.-L. Hartig, A. Ignatov, S. Ilieva,

S. Lalkovski, N. Mărginean, T. Otsuka, N. Shimizu, T. Togashi, and Y. Tsunoda, Phys. Rev. C **96**, 054323 (2017).
[27] Z. Bay, Phys. Rev. **77**, 419 (1950).
[28] J.-M. Régis, H. Mach, G. Simpson, J. Jolie, G. Pascovici, N. Saed-Samii, N. Warr, A. Bruce, J. Degenkolb, L. Fraile, C. Fransen, D. Ghita, S. Kisyov, U. Köster, A. Korgul, S. Lalkovski, N. Mărginean, P. Mutti, B. Olaizola, Z. Podolyak, P. Regan, O. Roberts, M. Rudigier, L. Stroe, W. Urban, and D. Wilmsen, Nucl. Instrum. Methods Phys. Res. A **726**, 191 (2013).
[29] J.-M. Régis, M. Rudigier, J. Jolie, A. Blazhev, C. Fransen, G. Pascovici, and N. Warr, Nucl. Instrum. Methods Phys. Res. A **684**, 36 (2012).
[30] P. C. Simms, N. Benczer-Koller, and C. S. Wu, Phys. Rev. **121**, 1169 (1961).
[31] V. Werner, N. Cooper, J.-M. Régis, M. Rudigier, E. Williams, J. Jolie, R. B. Cakirli, R. F. Casten, T. Ahn, V. Anagnostatou, Z. Berant, M. Bonett-Matiz, M. Elvers, A. Heinz, G. Ilie, D. Radeck, D. Savran, and M. K. Smith, Phys. Rev. C **93**, 034323 (2016).
[32] N. Nica, Nucl. Data Sheets **117**, 1 (2014).
[33] R. Lică, G. Benzoni, A. I. Morales, M. J. G. Borge, L. M. Fraile, H. Mach, M. Madurga, C. Sotty, V. Vedia, H. D. Witte, J. Benito, T. Berry, N. Blasi, A. Bracco, F. Camera, S. Ceruti, V. Charviakova, N. Cieplicka-Oryńczak, C. Costache, F. C. L. Crespi, J. Creswell, G. Fernández-Martínez, H. Fynbo, P. Greenlees, I. Homm, M. Huyse, J. Jolie, V. Karayonchev, U. Köster, J. Konki, T. Kröll, J. Kurcewicz, T. Kurtukian-Nieto, I. Lazarus, S. Leoni, M. Lund, N. Marginean, R. Marginean, C. Mihai, R. Mihai, A. Negret, A. Orduz, Z. Patyk, S. Pascu, V. Pucknell, P. Rahkila, J. M. Regis, F. Rotaru, N. Saed-Sami, V. Sánchez-Tembleque, M. Stanoiu, O. Tengblad, M. Thuerauf, A. Turturica, P. V. Duppen, and N. Warr, J. Phys. G: Nucl. Part. Phys. **44**, 054002 (2017).
[34] D. Bonatsos, D. Lenis, N. Minkov, P. P. Raychev, and P. A. Terziev, Phys. Rev. C **69**, 044316 (2004).
[35] D. D. Warner and R. F. Casten, Phys. Rev. Lett. **48**, 1385 (1982).
[36] D. D. Warner and R. F. Casten, Phys. Rev. C **28**, 1798 (1983).
[37] R. F. Casten, *Nuclear Structure from a Simple Perspective* (Oxford University Press, Oxford, 2000).
[38] J. Jolie, P. Cejnar, R. F. Casten, S. Heinze, A. Linnemann, and V. Werner, Phys. Rev. Lett. **89**, 182502 (2002).
[39] L. D. Landau and E. M. Lifshitz, *Statistical Physics, Course of Theoretical Physics*, Vol. V (Butterworth-Heinemann, Oxford, 2001).
[40] V. Werner, P. von Brentano, R. Casten, and J. Jolie, Phys. Lett. B **527**, 55 (2002).
[41] R. Casperson, Comput. Phys. Commun. **183**, 1029 (2012).
[42] E. Williams, R. J. Casperson, and V. Werner, Phys. Rev. C **82**, 054308 (2010).
[43] W.-T. Chou, N. V. Zamfir, and R. F. Casten, Phys. Rev. C **56**, 829 (1997).
[44] E. A. McCutchan, N. V. Zamfir, and R. F. Casten, Phys. Rev. C **69**, 064306 (2004).
[45] E. A. McCutchan and R. F. Casten, Phys. Rev. C **74**, 057302 (2006).
[46] P. Cejnar, J. Jolie, and R. F. Casten, Rev. Mod. Phys. **82**, 2155 (2010).
[47] A. J. Mitchell, C. J. Lister, E. A. McCutchan, M. Albers, A. D. Ayangeakaa, P. F. Bertone, M. P. Carpenter, C. J. Chiara, P. Chowdhury, J. A. Clark, P. Copp, H. M. David, A. Y. Deo, B. DiGiovine, N. D'Olympia, R. Dungan, R. D. Harding, J. Harker, S. S. Hota, R. V. F. Janssens, F. G. Kondev, S. H. Liu, A. V. Ramayya, J. Rissanen, G. Savard, D. Seweryniak, R. Shearman, A. A. Sonzogni, S. L. Tabor, W. B. Walters, E. Wang, and S. Zhu, Phys. Rev. C **93**, 014306 (2016).
[48] J. Dobaczewski, H. Flocard, and J. Treiner, Nucl. Phys. A **422**, 103 (1984).
[49] P. Klüpfel, P.-G. Reinhard, T. J. Bürvenich, and J. A. Maruhn, Phys. Rev. C **79**, 034310 (2009).
[50] P.-G. Reinhard, computer code SKYAX (unpublished).
[51] R. Fossion, D. Bonatsos, and G. A. Lalazissis, Phys. Rev. C **73**, 044310 (2006).
[52] M. Abolghasem, P. Alexa, A. Repko, and P.-G. Reinhard, Acta Phys. Pol. B **50**, 555 (2019).
[53] Z. P. Li, T. Nikšić, and D. Vretenar, J. Phys. G: Nucl. Part. Phys. **43**, 024005 (2016).